Giant magnetic response of a two-dimensional antiferromagnet

Lin Hao[1], D. Meyers[2], Hidemaro Suwa [ID]**[1,3], Junyi Yang[1], Clayton Frederick[1], Tamene R. Dasa[4], Gilberto Fabbris[2], Lukas Horak[5], Dominik Kriegner** [ID]**[5,6], Yongseong Choi[7], Jong-Woo Kim[7], Daniel Haskel[7], Philip J. Ryan[7,8], Haixuan Xu** [ID]**[4]*, Cristian D. Batista** [ID]**[1,9]*, M. P. M. Dean** [ID]**[2]* and Jian Liu** [ID]**[1]***

---

[1]Department of Physics and Astronomy, University of Tennessee, Knoxville, TN, USA. [2]Department of Condensed Matter Physics and Materials Science, Brookhaven National Laboratory, Upton, NY, USA. [3]Department of Physics, University of Tokyo, Tokyo, Japan. [4]Department of Materials Science and Engineering, University of Tennessee, Knoxville, TN, USA. [5]Department of Condensed Matter Physics, Charles University, Prague, Czech Republic. [6]Institute of Physics, Academy of Sciences of the Czech Republic, Prague, Czech Republic. [7]Advanced Photon Source, Argonne National Laboratory, Argonne, IL, USA. [8]School of Physical Sciences, Dublin City University, Dublin, Ireland. [9]Quantum Condensed Matter Division and Shull-Wollan Center, Oak Ridge National Laboratory, Oak Ridge, TN, USA. *e-mail: hxu8@utk.edu; cbatist2@utk.edu; mdean@bnl.gov; jianliu@utk.edu

1) Octahedral rotation pattern determined from DFT calculations

a $a^-a^-c^0$ **b** $a^0a^0c^-$

Top views

Side views
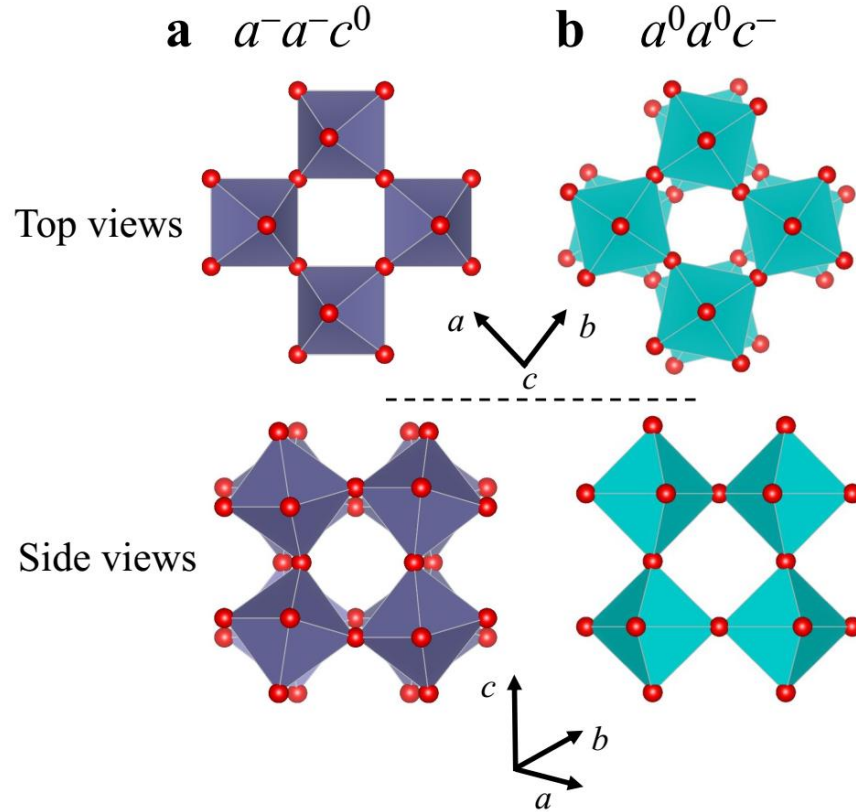
Figure S1 | **Schematic diagrams of Glazer notations $a^-a^-c^0$ (a) and $a^0a^0c^-$ (b).** A-site cations are omitted for clarity. The former represents a distorted lattice structure with out-of-phase octahedral rotations of the same amplitude along the a- and b-axes but no octahedral rotation along the c-axis. The latter denotes the presence of only an out-of-phase octahedral rotation along the c-axis.

Given the $a^-a^-c^-$ rotation pattern as found in the superlattice with single-layer SrTiO$_3$ spacer[1], we initialized the bi-layer-spaced superlattice with the same $a^-a^-c^-$ rotation pattern. All the internal atomic coordinates as well as the c-axis lattice parameter were relaxed during the geometry optimization until the force on each atom is less than 0.001 meV/Å. As shown in Fig. S2, we found

an almost straight Ir-O-Ti 179.75° out-of-plane bond angle. Therefore, the calculation result suggests an $a^0a^0c^-$ rotation pattern (Fig. S1b) in the present superlattice. To make sure the straight out-of-plane bond is not related to the specific choice of the initial structure, we initiated the lattice structure with various rotation patterns and rotation angles. Although there are slight changes in the c-axis lattice parameter, the straight out-of-plane bond is found to be robust and at 180° within the calculation accuracy of 0.5°.
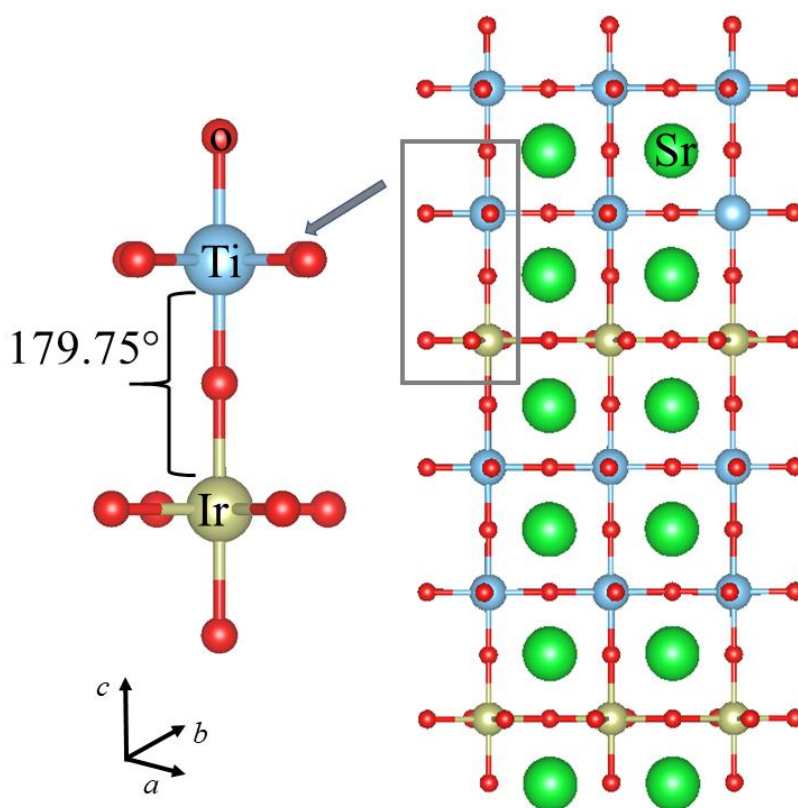
Figure S2 | Optimized lattice structure of the superlattice. An almost straight out-of-plane bond can be seen from the enlarged portion.

2) Experimental investigations of the lattice structure

Figure S3 summarized representative synchrotron XRD patterns at structural Bragg peaks characteristic of the octahedral rotations. As can be seen from Figs. S3a and b, no peak corresponding to in-phase rotation along the a-axis or the b-axis can be observed. Moreover, no observable film peak can be found at the (0.5 0.5 9.5) location, indicative of the absence of any out-of-phase rotation along the a-axis and the b-axis (Fig. S3c). In other words, all the planar oxygen ions remain in the same plane as the Ir sites, consistent with the DFT calculation. To verify the c-axis rotation pattern, we performed two L-scans along the (0.5 1.5 L) rod, covering multiple peak positions corresponding to in-phase and out-of-phase rotation around the c-axis (Figs. S3d and e). Note that the former (c^-) gives superlattice peaks at L = half-integer, while the latter (c^+) would create them at L = integer. Therefore, the presence of the half-integer peaks as well as the absence of any integer peaks unambiguously demonstrate a doubling of the unit cell along the c-axis. The rotation pattern of the present superlattice can then be identified as $a^0a^0c^-$ in Glazer notation[2,3].
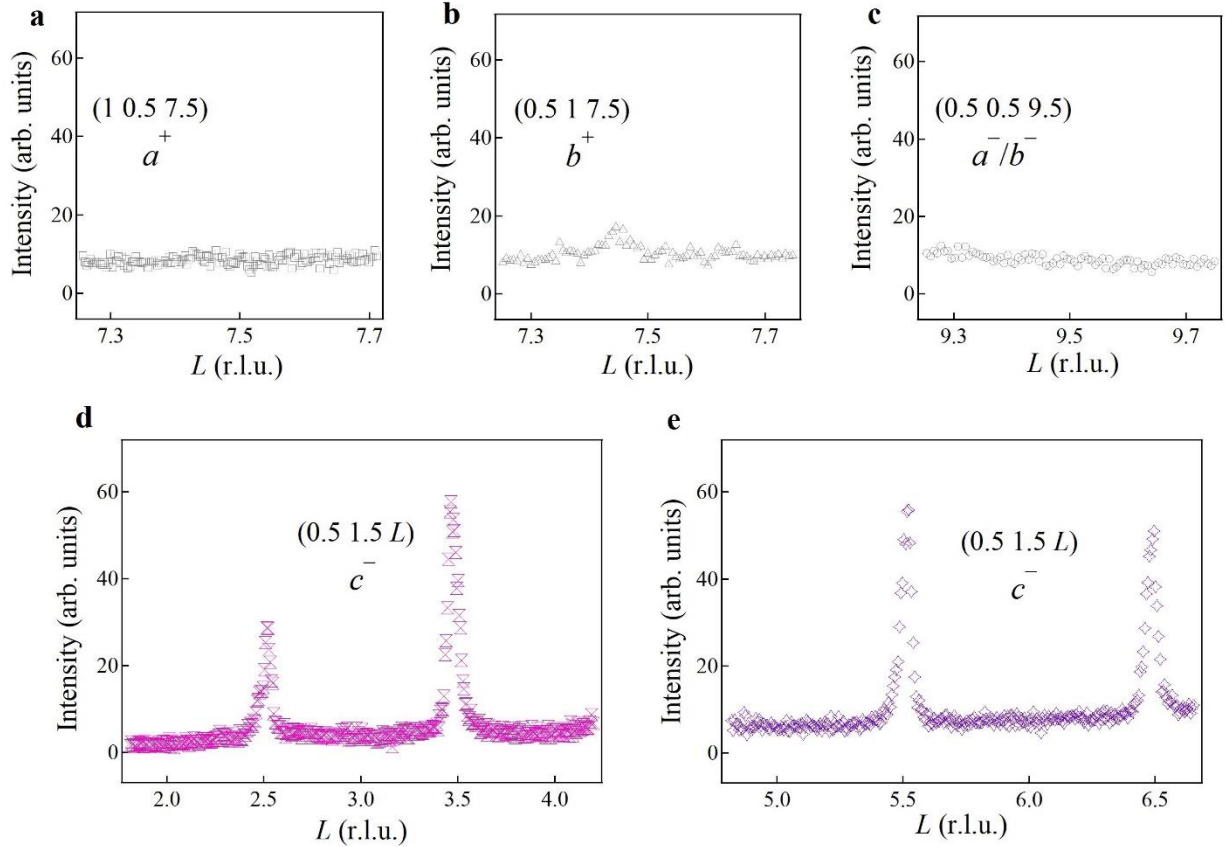
Figure 3 | **Synchrotron XRD measurements.** XRD patterns around the (1 0.5 7.5) (**a**), (0.5 1 7.5) (**b**) and (0.5 0.5 9.5) (**c**) reflections. **d** and **e** L-scans along the (0.5 1.5 L) truncation rod. The peak intensity is proportional to the squared of the corresponding rotation amplitude[3].

3) Confirmation of the $J_{eff} = 1/2$ state

As shown in Fig. S4, a strong absorption peak located at energy of 11.22 keV, evidences the Ir valence state of 4+[4]. Around the absorption edge, a clear XMCD signal can be seen, implying the dominant contribution of Ir ion to the total magnetic moment. Contrary to the finite XMCD peak around the L_3 edge, there is no observable XMCD signal at the L_2 edge within the experimental error. Note that the electron excitation from a $2p_{1/2}$ state to a $J_{eff} = 1/2$ state is

symmetry-forbidden[5,6]. The absence of XMCD intensity at L_2 edge here validates the notion of the

$J_{eff} = 1/2$ state, which can be described as pseudospin one-half, in the present superlattice[5].
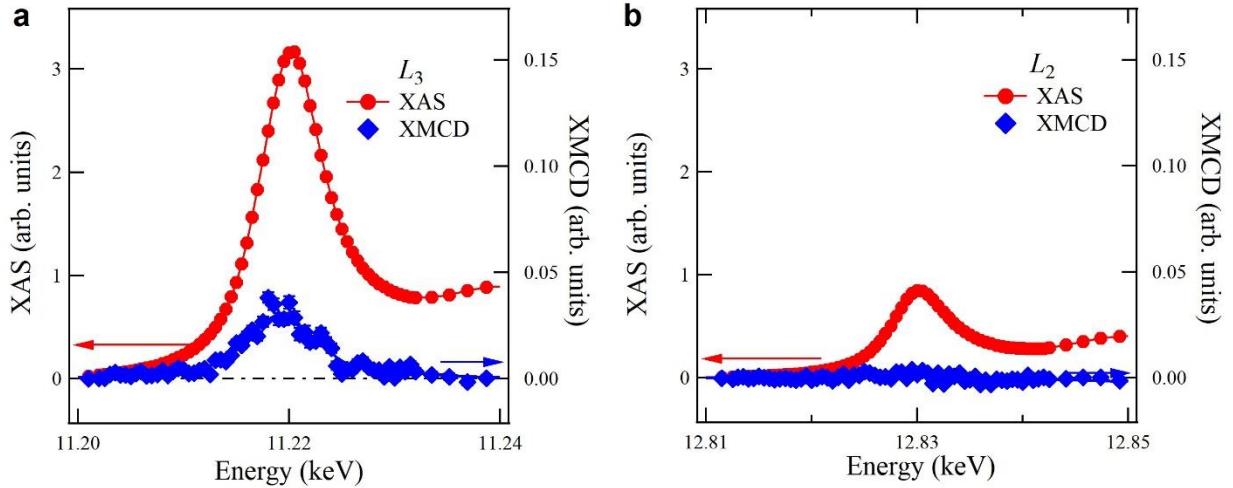
Figure S4 | XAS spectroscopy and XMCD measurements. Data were recorded around the Ir L_3 (**a**) and L_2 (**b**) edges at $T = 10$ K and magnetic field of 1 T. Magnetic field related artifacts in XMCD were eliminated by averaging signals after having reversed the magnetic field direction.

4) Magnetic resonance around the Ir L_3-edge.

Figure S5 displays an energy scan of the magnetic Bragg peak across the Ir L_3-edge, which shows a characteristic resonant profile of Ir moment[7]. Results shown in the main text were all taken with a photon energy corresponding to the resonant peak.
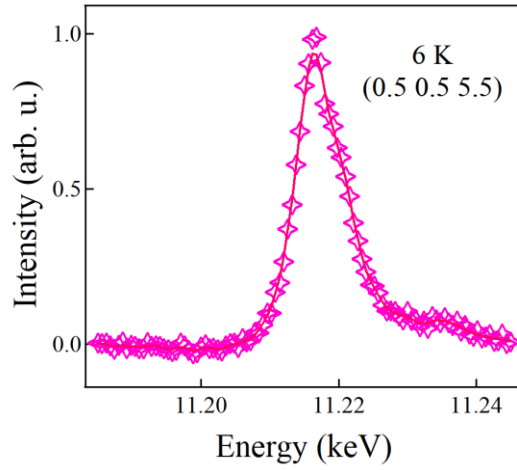
Figure S5 | Energy scan of the (0.5 0.5 5.5) magnetic Bragg peak around the Ir L_3 edge at 6 K.

5) Theoretical calculation on non-SU(2)-invariant exchange interaction models
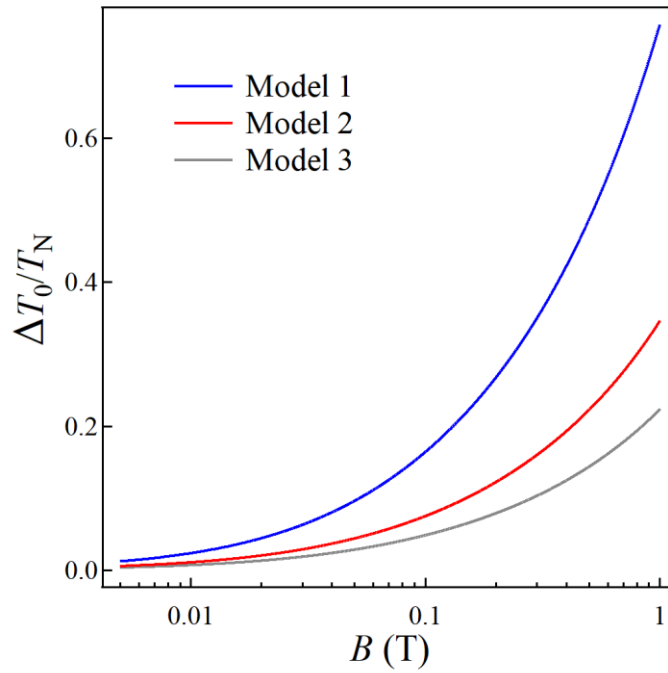
Figure S6. Comparison between the relative enhancement of T_0 as a function of magnetic field for model 1, 2, and 3: the quasi-SU(2)-invariance (blue), the non-SU(2)-invariance (red), and the XY-limit (grey).

References

1   Meyers, D. *et al.* Magnetism in artificial Ruddlesden-Popper iridates leveraged by structural distortions. Preprint at https://arxiv.org/abs/1707.08910 (2017).

2   Glazer, A. M. The classification of tilted octahedra in perovskites. *Acta Crystallogr. B, Struct. Crystallogr. Cryst. Chem.* **B28**, 3384-3392 (1972).

3   Glazer, A. M. Simple ways of determining perovskite structures. *Acta Cryst.* **A31**, 756-762 (1975).

4   Kim, B. J. *et al.* Phase-Sensitive Observation of a Spin-Orbital Mott State in Sr_2IrO_4. *Science* **323**, 1329-1332 (2009).

5   Jackeli, G. & Khaliullin, G. Mott Insulators in the Strong Spin-Orbit Coupling Limit: From Heisenberg to a Quantum Compass and Kitaev Models. *Phys. Rev. Lett.* **102**, 017205 (2009).

6   Haskel, D. *et al.* Pressure Tuning of the Spin-Orbit Coupled Ground State in Sr_2IrO_4. *Phys. Rev. Lett.* **109**, 027204 (2012).

7   Hao, L. *et al.* Two-Dimensional J_{eff}=1/2 Antiferromagnetic Insulator Unraveled from Interlayer Exchange Coupling in Artificial Perovskite Iridate Superlattices. *Phys. Rev. Lett.* **119**, 027204 (2017).